The Single-Finger Nucleocapsid Protein of Moloney Murine Leukemia Virus Binds and Destabilizes the TAR Sequences of HIV-1 but Does Not Promote Efficiently Their Annealing†

Caroline Egelé,‡ Etienne Piémont,‡ Pascal Didier,‡ Damien Ficheux,§ Bernard Roques,|| Jean-Luc Darlix,⊥ Hugues de Rocquigny,‡ and Yves Mély*,‡

Département de Pharmacologie et Physico-Chimie des Interactions Cellulaires et Moléculaires, UMR 7175 CNRS, Faculté de Pharmacie, Université Louis Pasteur, Strasbourg 1, 74, Route du Rhin, 67401 Illkirch Cedex, France, IBCP, 7, passage du Vercors, 69367 Lyon Cedex 07, France, Département de Pharmacochimie Moléculaire et Structurale, INSERM U266, Faculté de Pharmacie, 4, Avenue de l'Observatoire, 75270 Paris Cedex 06, France, and LaboRétro, Unité de Virologie Humaine INSERM, IFR128, Ecole Normale Supérieure de Lyon, 46 allée d'Italie, 69364 Lyon, France

Received June 21, 2007; Revised Manuscript Received August 17, 2007

ABSTRACT: The retroviral nucleocapsid proteins (NCs) are small proteins with either one or two conserved zinc fingers flanked by basic domains. NCs play key roles during reverse transcription by chaperoning the obligatory strand transfers. In HIV-1, the first DNA strand transfer relies on the NCp7-promoted destabilization and subsequent annealing of the transactivation response element, TAR with its complementary cTAR sequence. NCp7 chaperone activity relies mainly on its two folded fingers. Since NCs with a unique zinc finger are encoded by gammaretroviruses such as the canonical Moloney murine leukemia virus (MoMuLV), our objective was to characterize, by fluorescence techniques, the binding and chaperone activities of the NCp10 protein of MoMuLV to the TAR sequences of HIV-1. The unique finger and the flanking 12−25 and 40−48 domains of NCp10 were found to bind and destabilize cTAR stem−loop almost as efficiently as the homologous NCp7 protein. The flanking domains were essential for properly positioning the finger and, notably, the Trp35 residue onto cTAR. Thus, the binding and destabilization determinants scattered on the two NCp7 fingers are encoded by the unique finger of NCp10 and its flanking domains. NCp10 also activates the cTAR/TAR annealing reaction, but less efficiently than NCp7, suggesting that the two NCp7 fingers promote in concert the rate-limiting nucleation of the duplex. Due to its ability to mimic NCp7, the simple structure of NCp10 might be useful to design peptidomimetics aimed at inhibiting HIV replication.

Retroviral nucleocapsid proteins (NCs[1]) are small basic nucleic-acid binding proteins generated by the cleavage of the Gag precursor (*1*−*3*). NCs contain either one or two copies of a highly conserved C-X_2-C-X_4-H-X_4-C zinc finger that binds zinc ions with high affinities (*4*−*7*). Moreover, the fingers were found to be similarly folded around the zinc ion, while their flanking sequences remain flexible (*8*−*15*).

Retroviral NCs play critical functions during the early and late steps of the viral life cycle (for a review, see (*16*−*20*). These multiple roles are largely mediated by the NC ability to bind the genomic RNA and direct the rearrangement of nucleic acid molecules into their most stable conformation (*21*, *22*). The so-called nucleic acid chaperoning properties of NC are essential during the conversion of the genomic RNA into proviral DNA by reverse transcriptase, notably to anneal the primer tRNA to the initiation site (PBS) and to direct the two cDNA strand transfers. Such chaperoning activities have been extensively studied in the case of an NC with two zinc fingers, namely, NCp7 of the complex retrovirus human immunodeficiency virus type-1 (HIV-1) (*23*−*32*). In the (−) strand DNA transfer reaction, the (−) strand strong-stop DNA (ss-cDNA) is translocated to the 3′ end of the genomic RNA. This transfer is mediated by the hybridization of the repeat R sequences of 96 nucleotides at the 3′ ends of the ss-cDNA and genomic RNA, respectively. In vitro, the stable stem−loop (SL) structure of the TAR sequence within R at the very 3′ end of the genomic RNA does not readily hybridize with the complementary cTAR sequence (Figure 1b) of the ss-cDNA in the absence of NCp7

† This work was supported by grants from the Agence Nationale de Recherches sur le SIDA (ANRS), Sidaction, and the European Community (TRIoH integrated project). C.E. was a fellow from the Ministère de la Recherche et des Technologies.

* Corresponding author. Tel: +33 (0)3 90 24 42 63. Fax: +33 (0)3 90 24 43 12. E-mail: mely@pharma.u-strasbg.fr.

‡ Département de Pharmacologie et Physico-Chimie des Interactions Cellulaires et Moléculaires, UMR 7175 CNRS, Faculté de Pharmacie, Université Louis Pasteur.

§ IBCP.

|| Département de Pharmacochimie Moléculaire et Structurale, INSERM U266, Faculté de Pharmacie.

⊥ LaboRétro, Unité de Virologie Humaine INSERM, IFR128, Ecole Normale Supérieure de Lyon.

[1] Abbreviations: RT, reverse transcriptase; HIV-1, human immunodeficiency virus type 1; NC, nucleocapsid protein; PBS, primer binding site; ssDNA, strong-stop DNA; TAR, transactivation response element; FCS, fluorescence correlation spectroscopy; SL, stem−loop; Rh6G, 6-carboxyrhodamine; DABCYL, 4-(4′-dimethylaminophenylazo)benzoic acid; Fl, 5(and 6)-carboxyfluorescein; TMR, 5(and 6)-carboxytetramethylrhodamine; FRET, fluorescence resonance energy transfer; MoMuLV, Moloney murine leukemia virus; XMRV, xenotropic MuLV-related virus; ED, extended duplex; ODN, oligonucleotide.

10.1021/bi7012239 CCC: $37.00
Published on Web 11/21/2007

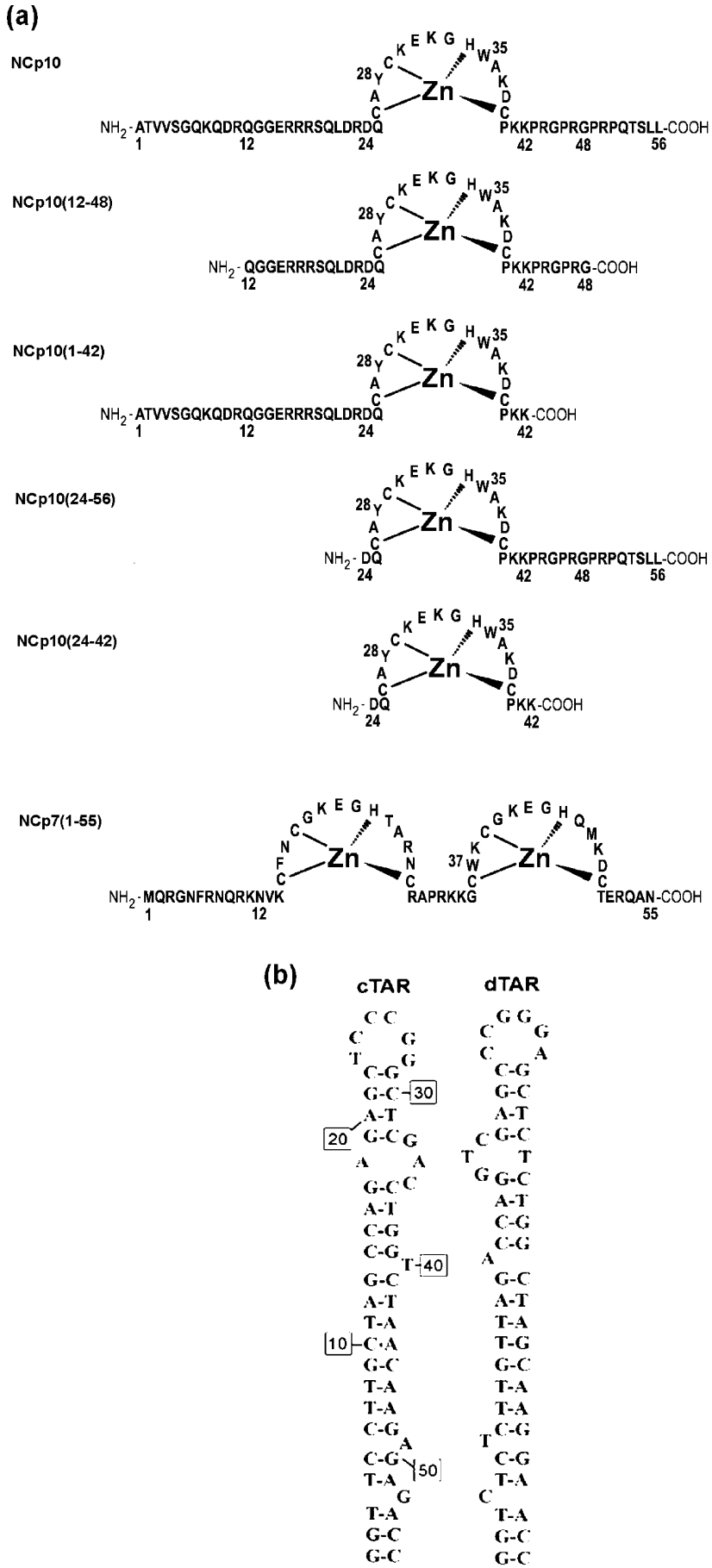

FIGURE 1: (a) Sequences of MoMuLV NCp10 and its deleted derivatives, and HIV-1 NCp7. (b) cTAR and dTAR sequences. The selected cTAR DNA sequence is the cDNA copy of the TAR RNA sequence from the MAL strain. The secondary structures of cTAR and dTAR derivatives were predicted from that of TAR and the mfold program (http://www.bioinfo.rpi.edu/applications/mfold/old/dna/form1.cgi).

(*23*, *26*−*28*, *30*, *32*). NCp7 chaperones ss-cDNA transfer by increasing the rate and extent of the annealing reaction (*24*, *30*, *32*−*35*) and by preventing nonspecific self-primed cDNA synthesis by RT (*26*−*29*, *34*, *36*).

The first mechanistic step of NCp7-assisted TAR/cTAR annealing corresponds to the destabilization of TAR and cTAR structures upon binding of NC molecules (*37*−*42*). NC activates the transient opening (fraying) of cTAR terminal base pairs leading to a partial melting (*37*, *39*) that propagates up to the middle of the stem (*40*, *42*−*44*). NC also melts TAR but less efficiency than cTAR. The two fingers in their proper context and the basic 29-RAPRKKG-35 linker fully support the NCp7 destabilizing activity (*43*). The folded finger domain is required for the formation of a hydrophobic platform at its surface that encompasses residues from both fingers. These residues and notably the Trp37 residue in the distal finger are essential for cTAR binding and melting (*12*, *43*, *45*, *46*). The second step in NC chaperoning of (−) strand transfer most probably corresponds to the NC-promoted invasion of the lower half of TAR stem by cTAR, leading to the final duplex (*40*, *44*, *47*). This step is likely promoted by the numerous basic residues in NC (Figure 1a) that may neutralize the charges of the DNA phosphates, thus decreasing the electrostatic repulsion between the oligonucleotides (*20*, *48*, *49*).

Simple retroviruses such as the murine leukemia virus (MuLV) have been instrumental in our understanding of retrovirus replication, retroviral-mediated gene transduction, and viral recombination (*50*−*52*). MuLV's belong to the family of gammaretrovirus (g-Retrovirus) and encode a small NC protein formed of a unique zinc finger flanked by highly basic sequences (*53*−*55*). Interestingly, a human gammaretrovirus similar to MuLV has recently been discovered to infect men with prostate cancer (*56*, *57*). In vitro experiments using a MuLV replication system have clearly shown that MuLV NCp10 chaperones the (−) strand transfer cDNA reaction (*58*, *59*) through the repeat R sequences of 68 nucleotides at the 3′ end of both the (-)ssDNA and the viral genome. As for HIV-1, the MuLV R sequence adopts a stable SL conformation (*60*, *61*) that is required for cDNA strand transfer (*58*). Interestingly, when the MuLV R sequences were replaced by that of HIV-1 in the MuLV context, but not by nonstructured sequences, NCp10 still chaperoned minus strand cDNA transfer (*59*). This indicates that (i) the chaperone activity of NCs is not strictly dependent on the homologous RNA, (ii) a SL structure is required (*58*), and (iii) NCp10 with a unique zinc finger can probably destabilize the stable TAR and cTAR sequences.

This prompted us to characterize in depth the binding and chaperoning activities of MuLV NCp10 on the stable TAR sequences of HIV-1 and to identify the structural determinants of these activities (Figure 1a). Results indicate that NCp10 binds cTAR with an affinity similar to that of NCp7 and destabilizes cTAR to an extent similar to that of NCp7 by activating the fraying of the cTAR termini. In addition, NCp10 activates the annealing kinetics of cTAR with its complementary sequence, but much less efficiently than NCp7. The NCp10 chaperone properties are mediated by its unique zinc finger and the flanking basic domains which are required for strong binding as well as for proper stacking of the Trp35 residue within TAR bases.

EXPERIMENTAL PROCEDURES

Materials. NCp10 derivatives (Figure 1a) were synthesized as previously described (*62*) and stored lyophilized in their zinc-bound form at −20 °C. Their purity was greater than 95%. Doubly labeled DNA oligonucleotides (ODNs) were synthesized at a 0.2 μmol scale by IBA GmbH Nucleic Acids Product Supply (Göttingen, Germany). The 5′ termini of the ODNs were labeled with either 6-carboxyrhodamine (Rh6G) or carboxytetramethylrhodamine (TMR) via an amino-linker with a six carbon spacer arm. The 3′ termini of the ODNs were labeled with either 4-(4′-dimethylaminophenylazo)-benzoic acid (DABCYL) or 5(and 6)-carboxyfluorescein (Fl) using a special solid support with the dye already attached. ODNs were purified by reverse-phase HPLC and polyacrylamide gel electrophoresis (PAGE). All experiments were performed at 20 °C in 25 mM Tris-HCl, pH 7.5, 30 mM NaCl, and 0.2 mM $MgCl_2$ (*30*).

UV−*Visible Absorption Spectroscopy.* Absorption spectra were recorded on a Cary 400 spectrophotometer. Extinction coefficients of 7000 M^{-1} cm^{-1} were used to determine the concentrations of the various NCp10 derivatives at 280 nm. The concentrations of cTAR and dTAR, the DNA equivalent of TAR, were determined using extinction coefficients at 260 nm of 521,910 M^{-1} cm^{-1} and 515,070 M^{-1} cm^{-1}, respectively.

Steady-State and Time-Resolved Fluorescence Measurements. Fluorescence emission spectra and kinetic traces were recorded on a FluoroMax spectrofluorometer (Jobin Yvon) equipped with a thermostated cell compartment. Fluorescence titrations were performed by adding increasing cTAR concentrations to a fixed amount of NCp10 or one of its peptide. The binding stoichiometry was determined at peptide concentrations between 1.5 μM and 2 μM, while the binding constants were determined at peptide concentrations between 0.2 μM and 1.5 μM. Fluorescence intensities were corrected for dilution, buffer fluorescence, and screening effects due to the ODN absorbance at the 295 nm excitation wavelength. Binding curves were fitted with eq 3 of (*63*).

Kinetic measurements were performed in pseudo-first-order conditions by using dTAR concentrations at least 10-fold higher than the concentration of the labeled cTAR sequence (*47*). Excitation and emission wavelengths were 480 nm and 520 nm, respectively, to monitor the Fl fluorescence. Peptides were added at a nucleotide to peptide ratio $r = 5$, except for NCp10 where $r = 10$. The apparent rate constants k_{obs} and the amplitudes were determined from the kinetic data by including a dead-time correction t_0 to take into account the delay between the mixing of reactants and the start of the measurements. All fitting procedures were carried out with the Microcal Origin 6.1 software based on the nonlinear, least-squares method and the Levenberg−Marquardt algorithm.

Time-resolved fluorescence measurements were performed with a time-correlated single photon counting technique as previously described (*64*). For NCp10 derivatives, the excitation and emission wavelengths for Trp were set at 295 and 350 nm, respectively. For TMR-5′-cTAR-3′-Fl, the excitation and emission wavelengths for Fl were set at 470 and 520 nm, respectively. Time-resolved data analysis was performed by the maximum entropy method using the Pulse5 software (*65*). The mean lifetime $\langle\tau\rangle$ was calculated from

the fluorescence lifetimes, τ_i, and the relative amplitudes, α_i, by $\langle\tau\rangle = \sum_i \alpha_i \tau_i$. The population, α_0, of dark species in NCp10 derivatives was calculated by

$$\alpha_0 = 1 - \frac{\langle\tau\rangle_A}{\langle\tau\rangle_B \times R_m} \quad (1)$$

where $\langle\tau\rangle_A$ and $\langle\tau\rangle_B$ are the measured mean lifetimes in the absence and the presence of a given concentration of cTAR, respectively. The population of dark species in TMR-5′-cTAR-3′-Fl was calculated by the same equation with $\langle\tau\rangle_A$ and $\langle\tau\rangle_B$ being the mean lifetimes of the singly labeled cTAR-3′-Fl in the absence of peptide and the doubly labeled TMR-5′-cTAR-3′-Fl in the absence or the presence of peptide, respectively. R_m corresponds to the ratio of their steady-state fluorescence intensities.

Steady-state anisotropy measurements were performed with a T-format SLM 8000 spectrofluorometer at 20 °C. The emitted light was monitored through high-pass filters (550 nm) (Kodak). A home-built device ensured the automatic rotation of the excitation polarizer. Anisotropy titrations were performed by adding increasing peptide concentrations to 100 nM 5′-Rh6G-cTAR. The Scatchard equation was rewritten to fit the anisotropy, *r*, as follows:

$$r = r_0 + \frac{(r_f - r_0)}{n}\left\{\frac{[1 + K_{app}(nN_t + L_t)]}{2K_{app}N_t} - \frac{\sqrt{[1 + K_{app}(nN_t + L_t)]^2 - 4nK_{app}{}^2N_tL_t}}{2K_{app}N_t}\right\} \quad (2)$$

where L_t and N_t designate the total concentration of peptide and 5′-Rh6G-cTAR, respectively. r_f represents the anisotropy at the plateau when all the peptide is bound, whereas r_0 and *r* correspond to the anisotropy values of 5′-Rh6G-cTAR in the absence and in the presence of a given concentration of NC, respectively. K_{app} and *n* correspond to the apparent binding constant and the number of protein binding sites, respectively. The numbers of binding sites were those calculated from the steady-state fluorescence titrations.

FCS Setup and Data Analysis. FCS measurements were performed on a two-photon platform including an Olympus IX70 inverted microscope (*37*, *66*). Two photon excitation at 850 nm is provided by a mode-locked Tsunami Ti:sapphire laser pumped by a Millenia V solid-state laser (Spectra Physics). The measurements were carried out in an 8 well Lab-Tek II coverglass system, using a 400 μL volume per well. For an ideal case of freely diffusing monodisperse fluorescent particles undergoing triplet blinking in a Gaussian excitation volume, the correlation function, $G(\tau)$, calculated online by an ALV-5000E correlator (ALV, Germany) from the fluorescence fluctuations can be fitted according to (*67*):

$$G(\tau) = \frac{1}{N}\left(1 + \frac{\tau}{\tau_{da}}\right)^{-1}\left(1 + \frac{1}{s^2}\frac{\tau}{\tau_{da}}\right)^{-1/2} \times \left(1 + \left(\frac{f_t}{1 - f_t}\right)\exp(-\tau/\tau_t)\right) \quad (3)$$

where τ_{da} is the apparent diffusion time (a parameter that is inversely related to the diffusion constant of the molecule), *N* is the mean number of molecules within the sample volume, *s* is the ratio between the axial and lateral radii of the sample volume, f_t is the mean fraction of fluorophores in their triplet state and τ_t is the triplet state lifetime. The excitation volume is about 0.3 μm^3, and *s* is about 3. Typical data recording times are 10 min.

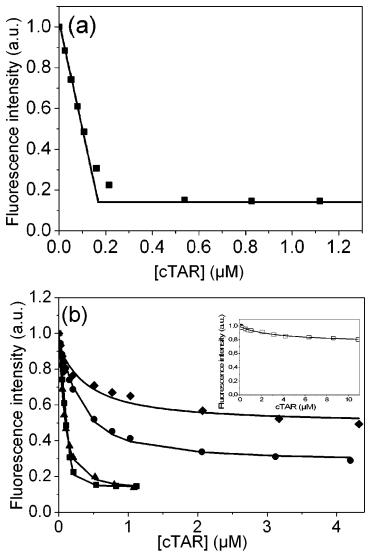

FIGURE 2: Binding curves of NCp10 derivatives with cTAR, as revealed by steady-state fluorescence. (a) Determination of the binding stoichiometry. The intercept of the initial slope with the plateau gives the number of NCp10 binding sites on cTAR. (b) Determination of the apparent binding constants. The concentrations of NCp10 (■), NCp10(12−48) (▲), NCp10(1−42) (●), NCp10(24−56) (◆), and NCp10(24−42) (□) (inset) were 1.5 μM in 25 mM Tris, 30 mM NaCl, and 0.2 mM $MgCl_2$, pH 7.5. Fluorescence intensities are expressed in arbitrary units. Excitation and emission wavelengths were 295 and 350 nm, respectively. The concentrations of cTAR are expressed in strands. Solid lines correspond to the fit of the experimental points with eq 3 of (*63*) and the parameters of Table 1.

RESULTS

Binding of MuLV NCp10 Protein and Peptides to the cTAR Stem−Loop Structure. We first characterized the binding of MoMuLV NCp10 to the multifunctional cTAR sequence of HIV-1 (*20*). To this end, reverse titrations (Figure 2) were performed by adding increasing ODN concentrations to a fixed NCp10 concentration in a 25 mM Tris pH 7.5, 30 mM NaCl, 0.2 mM $MgCl_2$ buffer which is currently used for evaluating NC destabilizing properties (*64*, *68*, *69*). Binding was monitored through the about 90% decrease of the Trp35 intrinsic fluorescence that accompanies the binding of cTAR SL (Table 1). This dramatic fluorescence quenching is in line with that observed in the NCp10−d(ACGCC) complex (*70*) and the complexes of NCp7 with various target ODNs, including cTAR (*38*, *71*−*73*). This strong quenching indicates stacking interactions between Trp35 of NCp10 and bases of the cTAR SL. To confirm this, time-resolved fluorescence experiments were performed. As previously reported (*6*), the intensity decay of the free NCp10 protein was characterized by two lifetimes, with a long-lived lifetime of 7.04 ns that represents 71% and a shorter lifetime of 2.44 ns (Table 2). Addition of a saturating amount of cTAR resulted in the appearance of two additional shorter lifetimes (0.17 ns and 1.43 ns) as well as a 3.9-fold decrease of the average lifetime $\langle\tau\rangle$. This decrease in $\langle\tau\rangle$ is significantly less than the 10-fold decrease in the steady-state fluorescence intensities, pointing to the existence of dark species with very

Table 1: Binding Parameters of NC Derivatives to cTAR[a]

	n[b]	b[c]	K_{app} (M^{-1})[d]	K_{app} (M^{-1})[e]	I_t/I_0 (%)[f]	ΔG (kcal/mol)
NCp7[g]	7.8 ± 0.4	7	(1 ± 0.2) × 10^8	nd[h]	8 ± 2	−10.7
NCp7(12−55)[g]	7.6 ± 0.6	7.2	(1.7 ± 0.2) × 10^7	nd	10 ± 3	−9.7
NCp10	8 ± 1	7.0	(2.3 ± 0.9) × 10^7	(2.5 ± 0.5) × 10^7	10 ± 4	−9.8 ± 0.3
NCp10(12−48)	7 ± 1	7.6	(4.2 ± 0.5) × 10^6	(1.8 ± 0.1) × 10^6	10 ± 4	−8.9 ± 0.1
NCp10(1−42)	6.7 ± 0.6	8.3	(2.0 ± 0.9) × 10^6	(8.4 ± 0.9) × 10^5	26 ± 6	−8.4 ± 0.3
NCp10(24−56)	8.0 ± 0.6	6.9	(2.6 ± 1.0) × 10^5	(2.1 ± 0.2) × 10^5	58 ± 7	−7.3 ± 0.2
NCp10(24−42)	18[i]	3.1	(1.6 ± 0.1) × 10^4	nd	80 ± 4	−5.7 ± 0.1

[a] Experiments were performed in 25 mM Tris, 30 mM NaCl, 0.2 mM $MgCl_2$, pH 7.5. [b] The number of binding sites was determined as described in the legend to Figure 2a. [c] The occluded binding site was calculated by dividing the number of cTAR nucleotides by n. [d] The K_{app} values were calculated by fitting the steady-state fluorescence data in Figure 2b to eq 3 of (*63*) and fixing the number of binding sites to its closest integer. [e] The K_{app} values were calculated by fitting the anisotropy data in Figure 3 to eq 2. [f] I_0 and I_t designate the fluorescence intensities of the peptide in the absence and presence of an excess of cTAR, respectively. [g] Data from ref *43*. [h] Not determined. [i] For NCp10(24−42), 18 binding sites were used (*43*).

Table 2: Time-Resolved Fluorescence Parameters of the Intrinsic Fluorescence of NC Derivatives Free and Bound to cTAR[a]

peptides	[cTAR] (μM)	α_0	τ_1 (ns)	α_1	τ_2 (ns)	α_2	τ_3 (ns)	α_3	τ_4 (ns)	α_4	$\langle\tau\rangle$ (ns)	R_m
NCp10	−	0					2.44	0.29	7.04	0.71	5.71	−
	1	0.62	0.17	0.51	1.43	0.30	3.47	0.09	6.25	0.11	1.48	10
				(0.20)		(0.11)		(0.03)		(0.04)		
NCp10(12−48)	−	0			0.96	0.10	3.06	0.16	7.29	0.74	5.98	−
	3	0.54	0.16	0.50	0.78	0.24	2.69	0.19	7.30	0.07	1.28	10
				(0.23)		(0.11)		(0.09)		(0.03)		
NCp10(1−42)	−	0					2.05	0.48	6.92	0.52	4.58	−
	4	0.10	0.14	0.47			2.17	0.43	6.78	0.10	1.68	3
				(0.42)				(0.39)		(0.09)		
NCp10(24−56)	−	0			1.86	0.32			5.46	0.68	4.31	−
	4	0.25	0.11	0.22	1.86	0.27			5.58	0.51	3.37	1.7
				(0.17)		(0.20)				(0.38)		
NCp10(24−42)	−	0			1.68	0.45			5.58	0.55	3.83	−
	10	0.00	0.12	0.29	1.91	0.32			5.63	0.39	2.84	1.3
				(0.29)		(0.32)				(0.39)		

[a] Experiments were performed with 1.5 μM peptides in 25 mM Tris, 30 mM NaCl, 0.2 mM $MgCl_2$, pH 7.5. The lifetimes, τ_i, and relative amplitudes, α_i, are expressed as means for at least three experiments. The standard deviations are usually below 10% for the lifetimes and the amplitudes. R_m is ratio of the fluorescence of the peptide in the absence of cTAR to that in the presence of the indicated concentration of cTAR. The relative amplitude, α_0, of the dark species is calculated by eq 1. The amplitudes given in brackets were recalculated to take into account α_0.

short (<20 ps) or null lifetime with a relative amplitude α_0 of 62%. Both the dark species and the short-lived components are typical of stacking interactions (*74*). As for the Trp37 residue in the NCp7/ODN complexes (*71*, *73*), the stacked conformation of Trp35 is by far the major species in the NCp10/cTAR complexes, representing more than 90%.

Then, the binding stoichiometry was inferred from the intersection of the initial slope of the titration with the fluorescence plateau (Figure 2a). We obtain a number of binding sites, n, of about eight (Table 1), corresponding to an occluded binding site, b, of about 7 nucleotides per NC molecule, similar to that reported for NCp7 (*43*, *72*, *73*, *75*). The apparent binding constant, $K_{app,}$ was determined (Figure 2b) by assuming that NCp10 binding sites on cTAR are identical and independent. This approach was shown to be reasonable to compare the binding affinities of NCp7 peptides to cTAR and PBS mutants (*63*, *72*). The K_{app} value of NCp10 for cTAR (2.3 × 10^7 M^{-1}) was found to be only four times less than that of NCp7 (*43*). To confirm this value, a direct titration of Rh6G-labeled cTAR by increasing NCp10 concentrations was performed by fluorescence anisotropy (Figure 3 inset). By fitting the binding curve with eq 2, a K_{app} value of (2.5 ± 0.5) × 10^7 M^{-1} was obtained, in excellent agreement with the previous value.

To identify the major NCp10 determinants for binding to cTAR, several NCp10 deletion mutants were designed (Figure 1a). In NCp10(12−48), both the N- and C-terminal domains were partly truncated while most of the basic residues were kept. In NCp10(1−42) and NCp10(24−56), the C-terminal and the N-terminal domains were deleted, respectively. Finally, in NCp10(24−42), both terminal domains were deleted leaving only the finger motif. Interest-

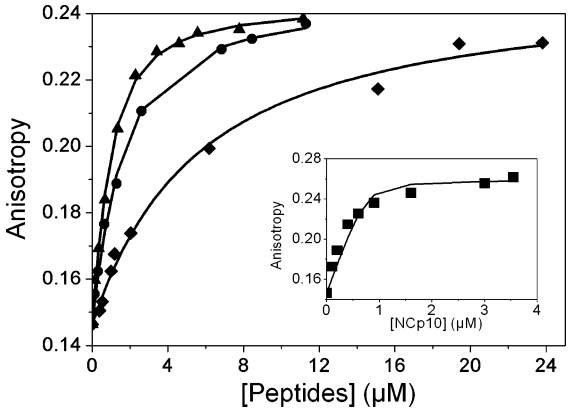

FIGURE 3: Binding curves of NCp10 derivatives with cTAR, as revealed by steady-state fluorescence anisotropy. The concentration of Rh6G-5′-cTAR was 100 nM. Anisotropy titrations were performed by adding increasing concentrations of NCp10 (■) (inset), NCp10(12−48) (▲), NCp10(1−42) (●), NCp10(24−56) (◆), in 25 mM Tris (pH 7.5), 30 mM NaCl, 0.2 mM $MgCl_2$. Excitation wavelength was 480 nm. Emission >550 nm was monitored through high-pass filters. Solid lines correspond to the fit of the experimental points with eq 2 and the parameters of Table 1.

ingly, both the fluorescence quenching and time-resolved fluorescence properties of the NCp10(12−48)/cTAR complex were close to those of the NCp10/cTAR complex (Figure 2b and Table 2), suggesting that the Trp35 residue was similarly stacked in both complexes. In addition, similar occluded binding sites and K_{app} values were found (Table 1), indicating that the deleted sequences only contributed to about 1 kcal/mol to the binding energy of NCp10 to cTAR. A more dramatic effect was observed when either the N- or the C-terminal domain was fully deleted. In both cases, the cTAR-induced quenching of Trp35 fluorescence was moderate, being 74% and 42% for NCp10(1−42) and NCp10(24−56), respectively. The population of dark and low-fluorescent species was below 55% (Table 2), indicating that Trp35 was stacked only in a limited fraction of these complexes. In the remaining complexes, the lifetimes were identical to those of the free peptide, suggesting that Trp35 did not interact with the bases of cTAR in such complexes. Though the occluded binding sites of both peptides were similar to that of NCp10, significant decreases were observed in their K_{app} values. Indeed, a 1 order of magnitude decrease in K_{app} was observed with NCp10(1−42), suggesting that the C-terminal (43−56) domain stabilizes the binding of NCp10 by ≈1.5 kcal/mol. A 2 orders of magnitude decrease in K_{app} was observed upon deleting the N-terminal (1−24) domain, indicating that this sequence stabilizes the NCp10 binding to cTAR by about 2.5 kcal/mol. The largest differences with the native NCp10 were observed with the NCp10(24−42) peptide, since the quenching of Trp 35 induced by its binding to cTAR was about 20%. This fluorescence decrease is mainly attributed to a short-lived lifetime (0.12 ns) that represents about 30%, indicating a partial stacking of Trp35 in a fraction of the complexes. Moreover, since the remaining lifetimes were identical to those of the free peptide, no stacking of Trp35 occurred in most complexes. Due to the low affinity of this peptide for cTAR, it was not possible to determine its binding stoichiometry. Assuming that its occluded binding site ($b = 3$) is similar to that of the isolated finger motifs of NCp7 (*7*, *43*), the K_{app} value was found to be about 3 orders of magnitudes smaller than that for NCp10. Thus, the basic N-terminal and C-terminal domains stabilize the binding of NCp10 by ≈4 kcal/mol, in full consistency with the sum of binding energies (1.5 kcal/mol + 2.5 kcal/mol) deduced separately from the NCp10(1−42) and NCp10-(24−56) mutants. Nevertheless, though the stabilization provided by the two terminal domains is significant, the major part of the binding energy of the NCp10/cTAR complex is conveyed by the finger motif that contributes to as much as 60% of the total binding energy at 30 mM NaCl.

Destabilization of the Stem−Loop Secondary Structure of cTAR by NCp10 Peptides. The nucleic acid destabilizing properties of NCp10 peptides were first characterized by using cTAR labeled at its 5′ and 3′ ends by Rh6G and DABCYL, respectively. The dyes form a nonfluorescent heterodimer when the SL is closed (*37*, *76*), while melting of the SL restores the Rh6G fluorescence. The melting potency of a given NCp10 peptide can thus be evaluated from the ratio of the fluorescence intensity in the presence versus the absence of the peptide (Table 3). Since the melting depends on the coating of cTAR by the peptide (*39*), the fraction, ν, of coated cTAR nucleotides (Table 3) was calculated from the binding constants (Table 1).

Table 3: Destabilization of cTAR by NC Derivatives, as Monitored from Steady-state Fluorescence Spectroscopy[a]

peptides	r	$I_{+peptide}/I_{-peptide}$	ν (%)	% Rh6G fluorescence restoration
NCp7[b]	5	6.9 ± 0.9	97	25
NCp7(12−55)[b]	5	6.9 ± 0.9	87	25
NCp10	5	7 ± 1	90	24 ± 2
NCp10(12−48)	5	7 ± 1	71	23 ± 3
	1	9.6 ± 0.8	95	36 ± 2
NCp10(1−42)	0.5	4.3 ± 0.7	96	14 ± 2
NCp10(24−56)	0.5	1.0 ± 0.2	73	0
NCp10(24−42)	0.5	1.00 ± 0.06	18	0

[a] Experiments were performed with 100 nM Rh6G-5′-cTAR-3′-DABCYL. r designates the ratio of nucleotides to peptide. The $I_{+peptide}/I_{-peptide}$ ratio designates the fluorescence intensity of the doubly labeled cTAR in the presence to that in the absence of peptide. Excitation and emission wavelengths are 480 and 550 nm, respectively. ν designates the fraction of cTAR nucleotides coated by the peptides, as calculated from Table 1. The restoration of the Rh6G fluorescence is calculated by assuming a 25-fold increase of fluorescence for the complete melting of the cTAR molecules. [b] Data from (*43*).

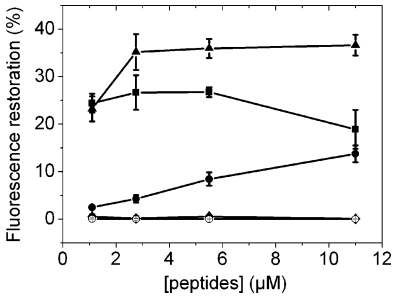

FIGURE 4: Restoration of Rh6G fluorescence in doubly labeled cTAR as revealed by steady-state fluorescence spectroscopy. The fluorescence intensity of 100 nM Rh6G-5′-cTAR3′-DABCYL was measured in the presence of NCp10 (■), NCp10(12−48) (▲), NCp10(1−42) (●), NCp10(24−56) (◆), and NCp10(24−42) (○) in 25 mM Tris, 30 mM NaCl, and 0.2 mM $MgCl_2$, pH 7.5. Restoration of Rh6G fluorescence was calculated by comparing the measured intensity to the intensities of the free cTAR and the fully melted one. Excitation wavelength was 480 nm.

Addition of NCp10 at a ratio r of 5 nucleotides per peptide caused a 7-fold increase of the fluorescence intensity of Rh6G-5′-cTAR-3′-DABCYL (Table 3), close to that observed with NCp7 (*39*, *43*). The similarities between NCp10 and NCp7 indicate that destabilization of cTAR can be achieved with a single finger motif. Since a full melting of cTAR would lead to a 25-fold increase of the Rh6G fluorescence, about 30% of the Rh6G fluorescence is restored upon NCp10 binding. At higher concentrations, NCp10 did not further increase the Rh6G fluorescence but rather decreased it (Figure 4), probably due to an aggregation of the NCp10/cTAR complexes, similar to that observed with the native NCp7 (*47*, *77*, *78*). This aggregation was confirmed by the sharp increase in the baseline of the absorption spectra due to light scattering (data not shown).

The truncated NCp10(12−48) mutant at $r = 5$ was found to increase the fluorescence intensity of Rh6G-5′-cTAR-3′-DABCYL to a level similar to NCp10, suggesting that the deletion mutant was as efficient as the native NCp10 with respect to this activity. Using higher concentrations of peptides (i.e., lower r values) to fully coat cTAR, the fluorescence restoration further increases up to ≈36% (Figure 4). The determinants of NCp10 destabilization activity are

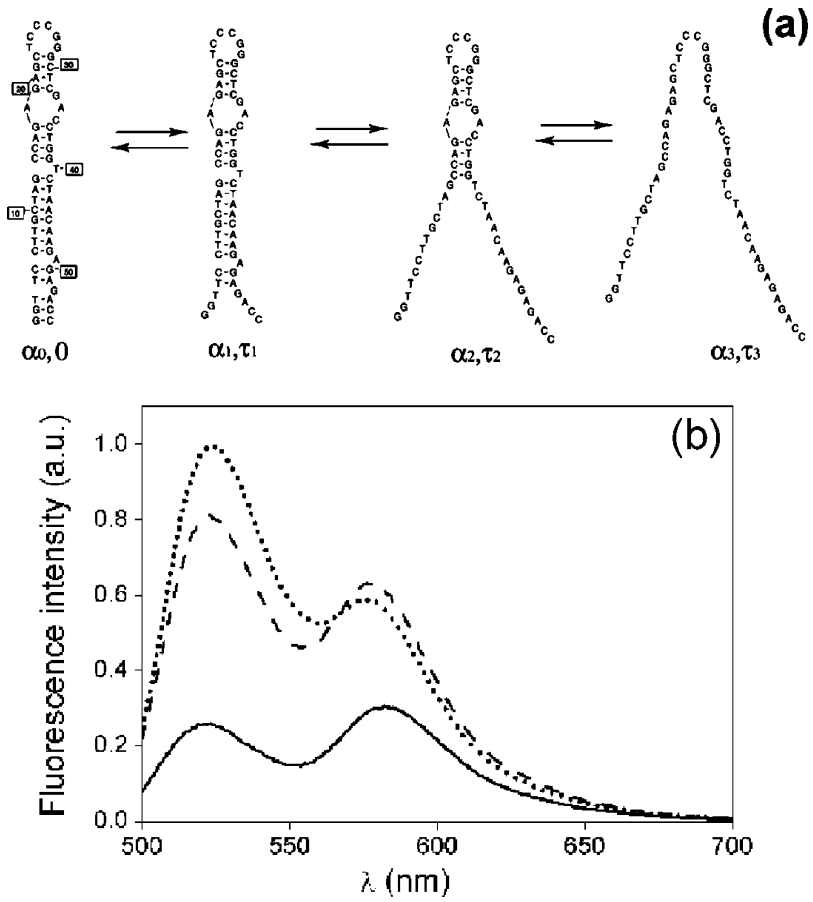

FIGURE 5: Fraying equilibrium of TMR-5′-cTAR-3′-Fl (a) and comparative effects of NCp10 and NCp7 on TMR-5′-cTAR-3′-Fl fluorescence spectrum (b). In (a), the equilibrium between the closed form and the various melted forms of TMR-5′-cTAR-3′-Fl has been drawn according to (*38*, *39*). The various forms are characterized by the lifetimes, τ_i, and relative populations, α_i, given in Table 4. (b) Effect of NCp10(12−48) and NCp7(12−55) on 100 nM TMR-5′-cTAR-3′-Fl as revealed by steady-state fluorescence spectroscopy. Excitation wavelength was 470 nm. Emission spectra were recorded either in the absence (solid line) or in the presence of NCp10(12−48) at $r = 1$ (dotted line) or NCp7(12−55) at $r = 5$ (dashed line).

thus within its (12−48) sequence, corresponding to the zinc finger and the flanking basic residues. Noticeably, the folding of the finger was found to be critical for cTAR destabilization since removal of zinc by an excess of EDTA prevented the peptide-promoted melting but not the binding to cTAR (data not shown).

Interestingly, a fluorescence restoration below 15% was observed with NCp10(1−42), even at concentrations where 95% of cTAR was coated by the peptide ($r = 0.5$), suggesting that the 43−48 sequence contains several determinants of NCp10 destabilizing activity. Furthermore, no destabilization of cTAR was observed with both NCp10(24−56) and NCp10(24−42) peptides, even at the highest tested concentrations. Thus, the finger alone or together with the C-terminal domain is unable to melt cTAR. Taken together, our data suggest that NCp10 determinants for its destabilizing activity are on the folded finger and its flanking (12−23) and (43−48) basic sequences.

To further characterize cTAR destabilization by MuLV NCp10, time-resolved fluorescence measurements with TMR-5′-cTAR-3′-Fl were performed. Though the Fl−TMR dye pair is less sensitive than the Rh6G−DABCYL pair, the time-resolved fluorescence decay of Fl is simpler than the Rh6G one and can be used to determine the extent of melting. Indeed, the three lifetime components, $\tau_1-\tau_3$, of Fl in TMR-5′-cTAR-3′-Fl can be associated with the melting of the terminal 3 bp segment, the lower half of cTAR, and the whole cTAR molecule, respectively (*38*, *39*) (Figure 5a). In addition, these partly melted species are in equilibrium with a population, α_0, of closed dark species (associated with a null lifetime) representing 81% (Table 4). NCp10(12−48) did not change the fluorescence lifetimes of TMR-5′-cTAR-3′-Fl but decreased the amplitudes associated with the less fluorescent species to the benefit of the most fluorescent ones (Table 4). Thus, like NCp7 and NCp7(12−55), NCp10(12−48) shifts the equilibrium toward the partly melted cTAR species. Interestingly, though the steady-state fluorescence intensities of TMR-5′-cTAR-3′-Fl complexed with NCp7 and NCp10(12−48) are similar, as can be seen from the R_m values (Table 4), significant differences appear in the amplitudes associated with the various lifetimes. Indeed, at comparable coating levels, NCp10(12−48) decreases less α_0 and increases less α_2 than NCp7, but increases more significantly the α_3 population associated with the full melting of cTAR. As a consequence, NCp10(12−48) shifts less than NCp7 finger domain the equilibrium from the closed to the partly melted cTAR species, but within the populations of melted species, NCp10(12−48) generates more efficiently the fully melted cTAR. The increased population of fully melted cTAR species induced by NCp10(12−48) as compared to NCp7(12−55) is further confirmed by the steady-state spectra of the two complexes (Figure 5b). Both the increased Fl peak

Table 4: Destabilization of cTAR by NC Derivatives, as Monitored by Time-Resolved Fluorescence[a]

	r	α_0	τ_1 (ns)	α_1	τ_2 (ns)	α_2	τ_3 (ns)	α_3	$\langle\tau\rangle$ (ns)	R_m
−	−	0.81	0.11	0.54	1.08	0.16	3.95	0.30	1.42	15
				(0.10)		(0.03)		(0.06)		
NCp7[b]	5	0.47	0.16	0.43	1.30	0.43	3.95	0.14	1.18	6.6
				(0.23)		(0.23)		(0.07)		
NCp7(12−55)[b]	5	0.46	0.15	0.33	1.39	0.37	3.76	0.30	1.69	4.5
				(0.18)		(0.20)		(0.16)		
NCp10(12−48)	5	0.62	0.16	0.27	1.07	0.29	3.67	0.44	1.97	5.3
				(0.10)		(0.11)		(0.17)		
	1	0.58	0.16	0.17	1.09	0.31	3.76	0.52	2.32	4.05
				(0.07)		(0.13)		(0.22)		
NCp10(24−56)	5	0.80	0.11	0.53	1.08	0.25	3.98	0.22	1.20	16.5
				(0.11)		(0.05)		(0.04)		

[a] Experimental conditions are as in Table 3. Parameter significance and expression are as in Table 2. R_m designates the ratio of the Fl fluorescence intensity of the singly labeled cTA*R*-3′-Fl derivative in the absence of peptide to that of the doubly labeled TMR-5′-cTA*R*-3′-Fl derivative in the absence or the presence of NC derivatives (*39*). The relative amplitude, α_0, of the dark species is calculated by eq 1 with $\langle\tau\rangle_{cTAR-3'-Fl} = 3.94$ ns. The amplitudes given in brackets were calculated as in Table 2. [b] Data from ref (*43*).

and the decreased TMR peak observed with NCp10(12−48) in comparison with NCp7(12−55) indicate a lower fluorescence resonance energy transfer and thus a larger distance between the two dyes, consistent with an increased melting of cTAR. The full melting of cTAR is highly sensitive to the coating level, as shown by the significantly lower α_3 value (0.17) for $\nu = 71\%$ ($r = 5$) as compared to the $\alpha_3 = 0.22$ value for $\nu = 95\%$ ($r = 1$). Finally, no change in the time-resolved parameters was observed with NCp10(24−56), confirming that this peptide does not modify the secondary structure of cTAR.

To further characterize the NCp10 promoted destabilization of cTAR, the kinetics of the transient openings (fraying) of cTAR stem terminus was investigated by fluorescence correlation spectroscopy (FCS). In this method, the fluorescence intensity arising from a very small volume containing a limited number of fluorescent molecules (about 12 molecules for a concentration of 100 nM) is correlated to obtain information about the processes that give rise to fluctuations in the fluorescence (*79*). The very small excitation volume (about 0.2 fL) is provided by two photon excitation. The dynamics of cTAR fraying were determined from the ratio $G^*(\tau)$ between the autocorrelation curve of the doubly labeled Rh6G-5′-cTAR-3′-DABCYL sequence to that of the singly labeled Rh6G-5′-cTAR sequence (Figure 6). For a two-state model between a fluorescent partly melted and a nonfluorescent closed SL, this ratio is expected to show a monoexponential decay: $G^*(\tau) = A + B\exp(-t/\tau_r)$ where B designates the amplitude, A is the limit value of $G^*(\tau)$, and τ_r is the reaction time (*37*, *38*, *80*). This allows then the deduction of the opening and closing rate constants describing stem terminus transient openings by

$$k_{op} = \tau_r^{-1}\frac{K_d}{1+K_d} \qquad k_{cl} = \tau_r^{-1}\frac{1}{1+K_d} \qquad (4)$$

where K_d is the equilibrium constant determined from time-resolved fluorescence measurements (Table 4).

In the absence of protein, the reaction time and calculated rate constants (Table 5) were very similar to those previously determined (*37*). NCp10(12−48) strongly reduced the reaction time, as shown by the much faster decay of $G^*(\tau)$ in its presence (Figure 6). This change in τ_r corresponded to a 19-fold increase in the k_{op} value and a 4-fold increase in the k_{cl} value, indicating that NCp10(12−48) strongly activates cTAR fraying. In sharp contrast, the reaction time and rate constants with NCp10(24−56) were indistinguishable from those of the free cTAR species, indicating that in line with its inability to destabilize cTAR, this peptide did not affect cTAR fraying.

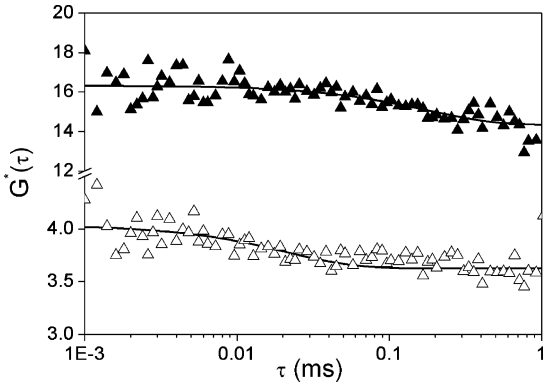

FIGURE 6: Dynamics of cTAR fraying as monitored by FCS. The ratio, $G^*(t)$, between the autocorrelation curves of 100 nM of Rh6G-5′-cTAR-3′-DABCYL and Rh6G-5′-cTAR was obtained either in the absence (▲) or in the presence (Δ) of 1.1 μM NCp10(12−48). The solid line is a three-parameter exponential fit to the data (see the text) with the parameters given in Table 5.

Table 5: Kinetics of cTAR Fraying[a]

peptides	r	τ_r (μs)	k_{op} (s^{-1})	k_{cl} (s^{-1})	K_d
−	−	180 ± 10	800 ± 30	4700 ± 200	0.17
NCp7(12−55)[b]	5	110 ± 20	4100 ± 800	5000 ± 1000	0.82
NCp10(12−48)	5	30 ± 10	15000 ± 7000	21000 ± 10000	0.68
NCp10(24−56)	5	230 ± 30	800 ± 100	3700 ± 400	0.22

[a] The chemical rate constants, τ_r, were deduced from the fits of the data in Figure 6 to $G^*(\tau) = A + B\exp(-t/\tau_r)$. The opening rate constants, k_{op}, and the closing rate constants, k_{cl}, were deduced from eq 4. The equilibrium constant K_d between open and closed cTAR species was determined from the time-resolved data of Rh6G-5′-cTAR-3′-DABCYL by $K_d = (1 - \alpha_0)/\alpha_0$. [b] Data from ref (*37*).

NCp10 Promotion of cTAR DNA/TAR DNA Annealing. The real-time annealing kinetics of cTAR with dTAR, the DNA analogue of the TAR sequence, was investigated by mixing TMR-5′-cTAR-3′-Fl with an excess of nonlabeled TAR DNA (dTAR). The less stable dTAR was preferred to TAR RNA since it allows faster annealing kinetics with less photobleaching. Formation of the 55 bp cTAR/dTAR extended duplex (ED) strongly increases the interchromophore

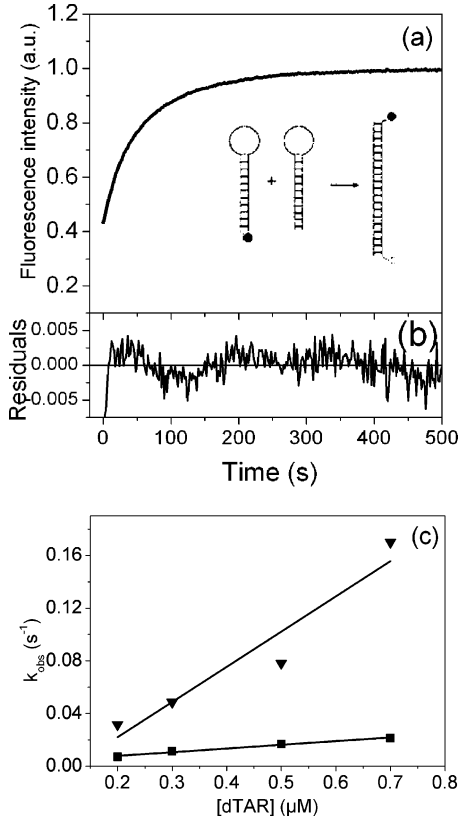

FIGURE 7: Promotion of cTAR/dTAR annealing by NCp10 derivatives. (a) Kinetic trace of 10 nM TMR-5′-cTAR-3′-Fl with 300 nM dTAR in the presence of NCp10 at $r = 10$ in 25 mM Tris-HCl (pH 7.5), 30 mM NaCl, 0.2 mM $MgCl_2$ at 20 °C. Excitation and emission wavelengths were 480 nm and 520 nm, respectively, to monitor the Fl emission. The solid line corresponds to the best fit to the data according to eq 5. Inset: Principle of the annealing reaction. Formation of the ED strongly increases the interchromophore distance and, thus, restores the Fl emission. (b) Residuals for a two-exponential fit of the experimental data. (c) Kinetic parameters of the cTAR/TAR annealing reaction in the presence of NCp10 at $r = 10$. The observed annealing rate constants for the fast (k_{obs1}) (▼) and slow (k_{obs2}) (■) components were determined in pseudo-first-order conditions and plotted as a function of the dTAR concentration. The solid line corresponds to the fit of the data with eq 6 and the k_{on} values given in Table 7. The k_{off} values are close to 0.

distance, leading to a full recovery of Fl emission (*47*). In the absence of NC protein, the cTAR/dTAR annealing was previously shown to involve two distinct kinetic components characterized by two slow second-order rate constants ($k_{on1} = 9000\ M^{-1}\ s^{-1}$ and $k_{on2} = 85\ M^{-1}\ s^{-1}$) (*47*). In the presence of NCp10, we observed the same fluorescence plateau as in the absence of protein, indicating that the reaction went to completion generating the ED (Figure 7a). Furthermore, NCp10 drastically increased the annealing kinetics, since the reaction was complete in less than 20 min, instead of more than 1 day in the absence of protein. The kinetic traces were adequately fitted (as could be seen by the nearly random distribution of the residuals around the zero value in Figure 7b) with a biexponential function:

$$I(t) = I_f - (I_f - I_0)(x\ e^{-k_{obs1}(t-t_o)} + (1-x)\ e^{-k_{obs2}(t-t_o)}) \quad (5)$$

where t_0 is the dead time, $k_{obs1,2}$ are the observed kinetic rate constants, x is the amplitude of the fast component, and I_0 and I_f are the fluorescence intensities of the SL and the ED, respectively. Both k_{obs} values varied linearly as a function of the dTAR concentration, suggesting that both kinetic components followed a second-order reaction (Figure 7c). The association ($k_{on1,2}$) and dissociation ($k_{off1,2}$) rate constants of both slow and fast components were determined according to

$$k_{obs1,2} = k_{on1,2}[dTAR] + k_{off1,2} \quad (6)$$

The k_{on1} value $(2.7 \pm 0.1) \times 10^5\ M^{-1}\ s^{-1}$ and k_{on2} value $(2.8 \pm 0.4) \times 10^4\ M^{-1}\ s^{-1}$ were respectively 1 and 2 orders of magnitude larger than the values of the corresponding rate constants in the absence of NC. Moreover, the k_{off} values were close to 0, indicating that the reverse reaction was negligible and, thus, that NCp10 can hardly melt the ED. The NCp10-promoted annealing of cTAR to dTAR is in line with the previously shown ability of NCp10 to chaperone the first strand cDNA transfer directed by HIV-1 R sequences (*59*). In further line with this last work, NCp10 was less efficient than NCp7, as could be seen from the 1 order of magnitude difference in their respective kinetic rate constants.

Table 6: Kinetic Parameters of cTAR-dTAR Annealing[a]

peptides	k_{on1} ($M^{-1}\ s^{-1}$)	k_{on2} ($M^{-1}\ s^{-1}$)
—[b]	9000 ± 800	85 ± 20
NCp7(12−55)[b]	$>10^6$	$(1.3 \pm 0.1) \times 10^5$
NCp10	$(2.7 \pm 0.1) \times 10^5$	$(2.8 \pm 0.4) \times 10^4$
NCp10(12−48)	$(1.4 \pm 0.1) \times 10^5$	$(2.0 \pm 0.3) \times 10^4$
NCp10(1−42)	$(1.6 \pm 0.2) \times 10^4$	$(1.5 \pm 0.1) \times 10^3$
NCp10(24−56)	$(2.5 \pm 0.4) \times 10^4$	$(3.4 \pm 0.1) \times 10^3$

[a] Peptides were used at $r = 5$, except for NCp10 which was used at $r = 10$. The kinetic rate constants for the fast (k_{on1}) and the slow (k_{on2}) components were calculated from the dependence of the k_{obs} values on the concentration of dTAR, as described in Figure 7. [b] Data from ref (*47*).

Interestingly, the annealing kinetics with the truncated NCp10(12−48) peptide was substantially the same as with NCp10 (Table 6), indicating that the terminal domains do not play a major role in the annealing reaction. In contrast, the NCp10(1−42) and NCp10(24−56) peptides were much less efficient in promoting cTAR/dTAR annealing since completion of the reaction required several hours in both cases. Values of the kinetic rate constants with both peptides were about 1 order of magnitude lower than those with NCp10 and NCp10(12−48). In fact, the annealing activities of both NCp10(1−42) and NCp10(24−56) are quite limited since both peptides only increase the k_{on1} and k_{on2} values by a factor of 2−3 and 15−40, respectively, in respect with the corresponding values in the absence of peptide. It can thus be concluded that the (12−23) and (43−48) sequences of NCp10 play a critical role in the annealing activation.

DISCUSSION

In the present study, we investigated the interaction of the MoMuLV NCp10 protein with the cTAR sequence of HIV-1 as well as the promotion by NCp10 of the cTAR/dTAR annealing. The affinity of NCp10 to cTAR was found to be of the same order of magnitude as that of the HIV-1 NCp7 protein and to be mainly supported by its (12−48) sequence. The major role of this sequence in the binding process is in line with NMR data showing that complexes of NCp10 with a fragment of the ψ RNA packaging signal and NCp10(14−

53) with dACGCC are stabilized by hydrophobic contacts involving residues Ala27, Tyr28, Trp35, and Ala36 from the finger domain, and also Leu21 and Pro43, located on both sides of the CCHC box (*70*, *81*, *82*). Moreover, the strong fluorescence decrease of the Trp35 residue indicates that, as for the UCUG sequence of ψ RNA (*81*, *82*), ACGCC (*70*), and polyU (*83*), Trp35 stacking with cTAR bases is critical for strong binding. The complex is likely further stabilized by interactions between the positively charged residues surrounding the zinc finger and the nucleotide backbone. The role of the domains flanking the central zinc finger as well as the importance of Trp35 stacking was confirmed by the strong affinity decrease and concomitant loss of Trp35 stacking observed with the deletion mutants (Table 1). Consequently, the role of the domains flanking the NCp10 finger might be to properly position the protein on its nucleic targets for optimal stacking of the Trp35 residue. Noticeably, the NCp10(12−48) domain appears comparable to the NCp7(12−55) domain, since both domains contribute at 30 mM NaCl to about 90% of the binding energy of their respective native proteins (Table 1). Thus, the binding determinants on the finger and the flanking domains of NCp10 appear similar to the determinants scattered on the two fingers and the basic linker of NCp7. In addition, the poor binding of the terminal (1−11) and (49−56) residues to cTAR is fully consistent with their limited interaction with ψRNA (*81*, *82*).

Moreover, NCp10 was found to shift the equilibrium of cTAR conformations to partly melted forms. NCp10 decreases less than NCp7 the population of closed cTAR species but generates more efficiently the fully melted form, probably due to its faster fraying kinetics (Table 5). The destabilizing activity of NCp10 is mainly supported by its central (12−48) domain that plays thus the same role as the central two finger domain of NCp7. This indicates that the destabilization activity does not require two fingers but can be mediated by one folded finger flanked by two basic domains. The critical importance of NCp10 folding in its chaperone properties may partly explain the loss of infectivity of MoMuLV virions where the Cys and His residues that bind zinc were mutated (*84*, *85*). Indeed, mutations of His34 to Cys or Cys39 to His were reported to affect reverse transcription and prevent the synthesis of full-length viral DNA (*86*). Similar mutations in NCp7 lead to misfolded fingers (*87*, *88*) that prevent the formation of the hydrophobic platform required for appropriate recognition and destabilization of SLs (*43*, *89*). In NCp10, this hydrophobic platform is thought to be formed by Trp35 and the nearly perfectly aligned residues Leu21, Ala27, and Ala36 residues (*70*). A clear relationship between the stacking of the Trp35 residue and cTAR destabilization was observed since the NCp10(24−56) and NCp10(24−42) mutants, that exhibit only a small population of stacked Trp residues, are unable to destabilize cTAR (Tables 2 and 3). Thus, by analogy to the Trp37 residue in NCp7, the stacking of Trp35 with the cTAR bases is critical for cTAR destabilization (*43*). The role of Trp35 in the destabilizing component of NCp10 chaperone activity together with its role in genomic RNA packaging may explain the loss of infectivity of MuLV virions where this residue has been mutated to Ser (*84*) or Gly (*85*). The inability of NCp10(24−56) and NCp10(24−42) to destabilize cTAR may also be related to the absence of the Leu21 residue that participates in the hydrophobic platform of NCp10 and forms hydrophobic contacts with dACGCC (*70*) and the UCUG binding sequence of ψRNA (*82*). Basic residues in the domains flanking the finger of NCp10 likely play also an important role in the destabilizing activity. Indeed, mutations of Arg16, Arg17, Arg18, Lys41, and Lys42 into neutral residues were shown to lead to poor DNA strand transfer and poorly infectious viruses (*55*, *59*). Our data with the NCp10(24−42) and NCp10(24−56) mutants (where Arg16 to 18 residues are missing) suggest that these basic residues strengthen the binding of NCp10 to cTAR and provide a proper orientation of its hydrophobic cleft for cTAR destabilization. Noticeably, the relative destabilizing properties of NCp10 and NCp7 are probably correlated with the stability of the target ODN sequence, since NCp10 was found to be far less efficient than NCp7 in destabilizing the long double-stranded sequence of the λ DNA (*90*).

The NCp10 and NCp10(12−48) peptides were also found to activate both the slow and fast kinetic components of the cTAR/dTAR annealing reaction. While only a moderate (1 order of magnitude) increase was observed for the fast component, previously associated with a limited annealing of the terminal bases of cTAR and dTAR (*47*), a 2 order of magnitude increase was observed for the slow component associated with the productive formation of the ED. These data indicate that the NCp10 annealing activity is also supported by the zinc finger and its flanking domains, in line with the critical role of these regions in primer annealing to the PBS (*54*, *55*, *59*, *85*, *86*). Interestingly, the cTAR/dTAR annealing kinetics with NCp10 is about 1 order of magnitude slower than with NCp7(12−55) (*47*) and about 2 orders of magnitude slower than with the full-length NCp7 (*44*). This slower activation as compared to NCp7 is in line with the lower ability of NCp10 to promote minus strand DNA transfer using HIV-1 R sequences (*59*). A still slower promotion of cTAR/dTAR annealing was observed with the truncated NCp10(1−42) and NCp10(24−56) peptides, probably due to their reduced ability to produce the reactive cTAR species where the lower half of the stem is melted (*44*, *47*). In this respect, the residual activity of the truncated mutants may be due to their ability to screen the repulsive electrostatic repulsion between the SLs and thus favor their encounter. In contrast to the truncated peptides, the reduced ability of the full-length NCp10 as compared to NCp7 to activate the annealing of cTAR with dTAR can hardly be attributed to differences in their destabilization properties, since the latter are comparable. Moreover, both NCp7 and NCp10 proteins being strongly positively charged, they screen probably to the same extent the negative charges of the SLs. In fact, the kinetically limiting step being the nucleation of the ED through the residues of the lower half of the SLs, the two fingers of NCp7 likely act in concert to facilitate this nucleation step. Alternatively, it cannot be excluded that NCp10 promotes cTAR/dTAR annealing by a different pathway, as for instance through a loop/loop interaction. This last pathway has also been evidenced with NCp7 (*40*, *91*, *92*), but as a minor one (*44*, *47*). Differences in the mechanisms of NCp7 and NCp10 are not unlikely since the SL in the cognate MoMuLV R sequence is shorter and less stable than the HIV TAR sequence (*60*).

In conclusion, the determinants of the chaperone activities scattered on the two fingers of NCp7 are encoded by the

single folded finger and the flanking domains of NCp10. The comparable destabilization of cTAR promoted by NCp10 and NCp7 may be attributed to their similar hydrophobic plateau. In NCp10, the flanking domains are likely critical for positioning the hydrophobic plateau onto the target ODN and notably, to allow an optimal stacking of Trp35 with the ODN bases. In contrast to cTAR destabilization, the promotion of cTAR/dTAR annealing was substantially less efficient with NCp10 than with NCp7, suggesting that two fingers are required for promoting the kinetically limiting nucleation of the ED. Nevertheless, due to its ability to bind strongly to TAR sequences and mimic NCp7 chaperone properties, the simpler structure of NCp10 could be used as a starting point to design peptidomimetics able to compete with NCp7 in the viral life cycle. Indeed, peptidomimetics based on a limited set of NCp7 structural determinants have previously been shown to impair reverse transcription and display antiviral activity (*93*). Similarly, these peptidomimetics might also be active against the protein region strictly homologous to the NCp10 sequence in the novel gammaretrovirus identified in prostate tumors (*56*, *57*).

ACKNOWLEDGMENT

We are grateful to E. Schaub and A. Hac for their help in FCS measurements.

REFERENCES

1. Henderson, L. E., Bowers, M. A., Sowder, R. C., 2nd, Serabyn, S. A., Johnson, D. G., Bess, J. W., Jr., Arthur, L. O., Bryant, D. K., and Fenselau, C. (1992) Gag proteins of the highly replicative MN strain of human immunodeficiency virus type 1: posttranslational modifications, proteolytic processings, and complete amino acid sequences, *J. Virol. 66*, 1856−1865.
2. Mervis, R. J., Ahmad, N., Lillehoj, E. P., Raum, M. G., Salazar, F. H., Chan, H. W., and Venkatesan, S. (1988) The gag gene products of human immunodeficiency virus type 1: alignment within the gag open reading frame, identification of posttranslational modifications, and evidence for alternative gag precursors, *J. Virol. 62*, 3993−4002.
3. Swanstrom, R., Wills, J. W. (2007) Synthesis, assembly and processing of viral proteins, *in Retroviruses*, (Coffin, M., Hugues, S. H. and Varmus, H. E., Ed), pp 263−334, Cold Spring Harbor Laboratory Press, Cold Spring Harbor, New York.
4. Green, L. M., and Berg, J. M. (1989) A retroviral Cys-Xaa2-Cys-Xaa4-His-Xaa4-Cys peptide binds metal ions: spectroscopic studies and a proposed three-dimensional structure, *Proc. Natl. Acad. Sci. U.S.A. 86*, 4047−4051.
5. Mely, Y., De Rocquigny, H., Morellet, N., Roques, B. P., and Gerard, D. (1996) Zinc binding to the HIV-1 nucleocapsid protein: a thermodynamic investigation by fluorescence spectroscopy, *Biochemistry 35*, 5175−5182.
6. Mely, Y., de Rocquigny, H., Piemont, E., Demene, H., Jullian, N., Fournie-Zaluski, M. C., Roques, B., and Gerard, D. (1993) Influence of the N- and C-terminal chains on the zinc-binding and conformational properties of the central zinc-finger structure of Moloney murine leukaemia virus nucleocapsid protein: a steady-state and time-resolved fluorescence study, *Biochim. Biophys. Acta 1161*, 6−18.
7. Mely, Y., Piemont, E., Sorinas-Jimeno, M., de Rocquigny, H., Jullian, N., Morellet, N., Roques, B. P., and Gerard, D. (1993) Structural and dynamic characterization of the aromatic amino acids of the human immunodeficiency virus type I nucleocapsid protein zinc fingers and their involvement in heterologous tRNA-(Phe) binding: a steady-state and time-resolved fluorescence study, *Biophys. J. 65*, 1513−1522.
8. Demene, H., Jullian, N., Morellet, N., de Rocquigny, H., Cornille, F., Maigret, B., and Roques, B. P. (1994) Three-dimensional 1H NMR structure of the nucleocapsid protein NCp10 of Moloney murine leukemia virus, *J. Biomol. NMR 4*, 153−170.
9. Gao, Y., Kaluarachchi, K., and Giedroc, D. P. (1998) Solution structure and backbone dynamics of Mason-Pfizer monkey virus (MPMV) nucleocapsid protein, *Protein Sci. 7*, 2265−2280.
10. Kodera, Y., Sato, K., Tsukahara, T., Komatsu, H., Maeda, T., and Kohno, T. (1998) High-resolution solution NMR structure of the minimal active domain of the human immunodeficiency virus type-2 nucleocapsid protein, *Biochemistry 37*, 17704−17713.
11. Morellet, N., de Rocquigny, H., Mely, Y., Jullian, N., Demene, H., Ottmann, M., Gerard, D., Darlix, J. L., Fournie-Zaluski, M. C., and Roques, B. P. (1994) Conformational behaviour of the active and inactive forms of the nucleocapsid NCp7 of HIV-1 studied by 1H NMR, *J. Mol. Biol. 235*, 287−301.
12. Morellet, N., Demene, H., Teilleux, V., Huynh-Dinh, T., de Rocquigny, H., Fournie-Zaluski, M. C., and Roques, B. P. (1998) Structure of the complex between the HIV-1 nucleocapsid protein NCp7 and the single-stranded pentanucleotide d(ACGCC), *J. Mol. Biol. 283*, 419−434.
13. Morellet, N., Jullian, N., De Rocquigny, H., Maigret, B., Darlix, J. L., and Roques, B. P. (1992) Determination of the structure of the nucleocapsid protein NCp7 from the human immunodeficiency virus type 1 by 1H NMR, *EMBO J. 11*, 3059−3065.
14. Morellet, N., Meudal, H., Bouaziz, S., and Roques, B. P. (2006) Structure of the zinc finger domain encompassing residues 13−51 of the nucleocapsid protein from simian immunodeficiency virus, *Biochem. J. 393*, 725−732.
15. Summers, M. F., Henderson, L. E., Chance, M. R., Bess, J. W., Jr., South, T. L., Blake, P. R., Sagi, I., Perez-Alvarado, G., Sowder, R. C., 3rd, Hare, D. R., et al. (1992) Nucleocapsid zinc fingers detected in retroviruses: EXAFS studies of intact viruses and the solution-state structure of the nucleocapsid protein from HIV-1, *Protein Sci. 1*, 563−574.
16. Bampi, C., Jacquenet, S., Lener, D., Decimo, D., and Darlix, J. L. (2004) The chaperoning and assistance roles of the HIV-1 nucleocapsid protein in proviral DNA synthesis and maintenance, *Curr. HIV Res. 2*, 79−92.
17. Cimarelli, A., and Darlix, J. L. (2002) Assembling the human immunodeficiency virus type 1, *Cell. Mol. Life Sci. 59*, 1166−1184.
18. Cristofari, G., and Darlix, J. L. (2002) The ubiquitous nature of RNA chaperone proteins, *Prog. Nucleic Acid Res. Mol. Biol. 72*, 223−268.
19. Darlix, J. L., Lopez Lastra, M., Mély, Y., and Roques, B. (2002) Nucleocapsid protein chaperoning of nucleic acids at the heart of HIV structure, assembly and cDNA synthesis, in *Sequence HIV Compendium*, pp 69−88, Los Alamos National Laboratory, Los Alamos.
20. Levin, J. G., Guo, J., Rouzina, I., and Musier-Forsyth, K. (2005) Nucleic acid chaperone activity of HIV-1 nucleocapsid protein: critical role in reverse transcription and molecular mechanism, *Prog. Nucleic Acid Res. Mol. Biol. 80*, 217−286.
21. Herschlag, D. (1995) RNA chaperones and the RNA folding problem, *J. Biol. Chem. 270*, 20871−20874.
22. Rein, A., Henderson, L. E., and Levin, J. G. (1998) Nucleic-acid-chaperone activity of retroviral nucleocapsid proteins: significance for viral replication, *Trends Biochem. Sci. 23*, 297−301.
23. Baudin, F., Marquet, R., Isel, C., Darlix, J. L., Ehresmann, B., and Ehresmann, C. (1993) Functional sites in the 5′ region of human immunodeficiency virus type 1 RNA form defined structural domains, *J. Mol. Biol. 229*, 382−397.
24. Darlix, J. L., Vincent, A., Gabus, C., de Rocquigny, H., and Roques, B. (1993) Trans-activation of the 5′ to 3′ viral DNA strand transfer by nucleocapsid protein during reverse transcription of HIV1 RNA, *C. R. Acad. Sci., Ser. III 316*, 763−771.
25. De Rocquigny, H., Gabus, C., Vincent, A., Fournie-Zaluski, M. C., Roques, B., and Darlix, J. L. (1992) Viral RNA annealing activities of human immunodeficiency virus type 1 nucleocapsid protein require only peptide domains outside the zinc fingers, *Proc. Natl. Acad. Sci. U.S.A. 89*, 6472−6476.
26. Driscoll, M. D., and Hughes, S. H. (2000) Human immunodeficiency virus type 1 nucleocapsid protein can prevent self-priming of minus-strand strong stop DNA by promoting the annealing of short oligonucleotides to hairpin sequences, *J. Virol. 74*, 8785−8792.
27. Guo, J., Henderson, L. E., Bess, J., Kane, B., and Levin, J. G. (1997) Human immunodeficiency virus type 1 nucleocapsid protein promotes efficient strand transfer and specific viral DNA synthesis by inhibiting TAR-dependent self-priming from minus-strand strong-stop DNA, *J. Virol. 71*, 5178−5188.

28. Heilman-Miller, S. L., Wu, T., and Levin, J. G. (2004) Alteration of nucleic acid structure and stability modulates the efficiency of minus-strand transfer mediated by the HIV-1 nucleocapsid protein, *J. Biol. Chem. 279*, 44154−44165.
29. Lapadat-Tapolsky, M., Gabus, C., Rau, M., and Darlix, J. L. (1997) Possible roles of HIV-1 nucleocapsid protein in the specificity of proviral DNA synthesis and in its variability, *J. Mol. Biol. 268*, 250−260.
30. Lapadat-Tapolsky, M., Pernelle, C., Borie, C., and Darlix, J. L. (1995) Analysis of the nucleic acid annealing activities of nucleocapsid protein from HIV-1, *Nucleic Acids Res. 23*, 2434−2441.
31. Prats, A. C., Sarih, L., Gabus, C., Litvak, S., Keith, G., and Darlix, J. L. (1988) Small finger protein of avian and murine retroviruses has nucleic acid annealing activity and positions the replication primer tRNA onto genomic RNA, *EMBO J. 7*, 1777−1783.
32. You, J. C., and McHenry, C. S. (1994) Human immunodeficiency virus nucleocapsid protein accelerates strand transfer of the terminally redundant sequences involved in reverse transcription, *J. Biol. Chem. 269*, 31491−31495.
33. Davis, W. R., Gabbara, S., Hupe, D., and Peliska, J. A. (1998) Actinomycin D inhibition of DNA strand transfer reactions catalyzed by HIV-1 reverse transcriptase and nucleocapsid protein, *Biochemistry 37*, 14213−14221.
34. Guo, J., Wu, T., Anderson, J., Kane, B. F., Johnson, D. G., Gorelick, R. J., Henderson, L. E., and Levin, J. G. (2000) Zinc finger structures in the human immunodeficiency virus type 1 nucleocapsid protein facilitate efficient minus- and plus-strand transfer, *J. Virol. 74*, 8980−8988.
35. Guo, J., Wu, T., Bess, J., Henderson, L. E., and Levin, J. G. (1998) Actinomycin D inhibits human immunodeficiency virus type 1 minus-strand transfer in in vitro and endogenous reverse transcriptase assays, *J. Virol. 72*, 6716−6724.
36. Golinelli, M. P., and Hughes, S. H. (2003) Secondary structure in the nucleic acid affects the rate of HIV-1 nucleocapsid-mediated strand annealing, *Biochemistry 42*, 8153−8162.
37. Azoulay, J., Clamme, J. P., Darlix, J. L., Roques, B. P., and Mely, Y. (2003) Destabilization of the HIV-1 complementary sequence of TAR by the nucleocapsid protein through activation of conformational fluctuations, *J. Mol. Biol. 326*, 691−700.
38. Beltz, H., Azoulay, J., Bernacchi, S., Clamme, J. P., Ficheux, D., Roques, B., Darlix, J. L., and Mely, Y. (2003) Impact of the terminal bulges of HIV-1 cTAR DNA on its stability and the destabilizing activity of the nucleocapsid protein NCp7, *J. Mol. Biol. 328*, 95−108.
39. Bernacchi, S., Stoylov, S., Piemont, E., Ficheux, D., Roques, B. P., Darlix, J. L., and Mely, Y. (2002) HIV-1 nucleocapsid protein activates transient melting of least stable parts of the secondary structure of TAR and its complementary sequence, *J. Mol. Biol. 317*, 385−399.
40. Cosa, G., Zeng, Y., Liu, H. W., Landes, C. F., Makarov, D. E., Musier-Forsyth, K., and Barbara, P. F. (2006) Evidence for non-two-state kinetics in the nucleocapsid protein chaperoned opening of DNA hairpins, *J. Phys. Chem. B 110*, 2419−2426.
41. Hong, M. K., Harbron, E. J., O'Connor, D. B., Guo, J., Barbara, P. F., Levin, J. G., and Musier-Forsyth, K. (2003) Nucleic acid conformational changes essential for HIV-1 nucleocapsid protein-mediated inhibition of self-priming in minus-strand transfer, *J. Mol. Biol. 325*, 1−10.
42. Liu, H. W., Cosa, G., Landes, C. F., Zeng, Y., Kovaleski, B. J., Mullen, D. G., Barany, G., Musier-Forsyth, K., and Barbara, P. F. (2005) Single-molecule FRET studies of important intermediates in the nucleocapsid-protein-chaperoned minus-strand transfer step in HIV-1 reverse transcription, *Biophys. J. 89*, 3470−3479.
43. Beltz, H., Clauss, C., Piemont, E., Ficheux, D., Gorelick, R. J., Roques, B., Gabus, C., Darlix, J. L., de Rocquigny, H., and Mely, Y. (2005) Structural determinants of HIV-1 nucleocapsid protein for cTAR DNA binding and destabilization, and correlation with inhibition of self-primed DNA synthesis, *J. Mol. Biol. 348*, 1113−1126.
44. Liu, H. W., Zeng, Y., Landes, C. F., Kim, Y. J., Zhu, Y., Ma, X., Vo, M. N., Musier-Forsyth, K., and Barbara, P. F. (2007) Insights on the role of nucleic acid/protein interactions in chaperoned nucleic acid rearrangements of HIV-1 reverse transcription, *Proc. Natl. Acad. Sci. U.S.A. 104*, 5261−5267.
45. Amarasinghe, G. K., Zhou, J., Miskimon, M., Chancellor, K. J., McDonald, J. A., Matthews, A. G., Miller, R. R., Rouse, M. D., and Summers, M. F. (2001) Stem-loop SL4 of the HIV-1 psi RNA packaging signal exhibits weak affinity for the nucleocapsid protein. structural studies and implications for genome recognition, *J. Mol. Biol. 314*, 961−970.
46. De Guzman, R. N., Wu, Z. R., Stalling, C. C., Pappalardo, L., Borer, P. N., and Summers, M. F. (1998) Structure of the HIV-1 nucleocapsid protein bound to the SL3 psi-RNA recognition element, *Science 279*, 384−388.
47. Godet, J., de Rocquigny, H., Raja, C., Glasser, N., Ficheux, D., Darlix, J. L., and Mely, Y. (2006) During the early phase of HIV-1 DNA synthesis, nucleocapsid protein directs hybridization of the TAR complementary sequences via the ends of their double-stranded stem, *J. Mol. Biol. 356*, 1180−1192.
48. Williams, M. C., Rouzina, I., and Bloomfield, V. A. (2002) Thermodynamics of DNA interactions from single molecule stretching experiments, *Acc. Chem. Res. 35*, 159−166.
49. Williams, M. C., Rouzina, I., Wenner, J. R., Gorelick, R. J., Musier-Forsyth, K., and Bloomfield, V. A. (2001) Mechanism for nucleic acid chaperone activity of HIV-1 nucleocapsid protein revealed by single molecule stretching, *Proc. Natl. Acad. Sci. U.S.A. 98*, 6121−6126.
50. Coffin, J. M. (1979) Structure, replication, and recombination of retrovirus genomes: some unifying hypotheses, *J. Gen. Virol. 42*, 1−26.
51. Emerman, M., and Temin, H. M. (1986) Comparison of promoter suppression in avian and murine retrovirus vectors, *Nucleic Acids Res. 14*, 9381−9396.
52. Zhang, J., and Temin, H. M. (1994) Retrovirus recombination depends on the length of sequence identity and is not error prone, *J. Virol. 68*, 2409−2414.
53. Cornille, F., Mely, Y., Ficheux, D., Savignol, I., Gerard, D., Darlix, J. L., Fournie-Zaluski, M. C., and Roques, B. P. (1990) Solid phase synthesis of the retroviral nucleocapsid protein NCp10 of Moloney murine leukaemia virus and related "zinc-fingers" in free SH forms. Influence of zinc chelation on structural and biochemical properties, *Int. J. Pept. Protein Res. 36*, 551−558.
54. De Rocquigny, H., Ficheux, D., Gabus, C., Allain, B., Fournie-Zaluski, M. C., Darlix, J. L., and Roques, B. P. (1993) Two short basic sequences surrounding the zinc finger of nucleocapsid protein NCp10 of Moloney murine leukemia virus are critical for RNA annealing activity, *Nucleic Acids Res. 21*, 823−829.
55. Housset, V., De Rocquigny, H., Roques, B. P., and Darlix, J. L. (1993) Basic amino acids flanking the zinc finger of Moloney murine leukemia virus nucleocapsid protein NCp10 are critical for virus infectivity, *J. Virol. 67*, 2537−2545.
56. Dong, B., Kim, S., Hong, S., Das Gupta, J., Malathi, K., Klein, E. A., Ganem, D., Derisi, J. L., Chow, S. A., and Silverman, R. H. (2007) An infectious retrovirus susceptible to an IFN antiviral pathway from human prostate tumors, *Proc. Natl. Acad. Sci. U.S.A. 104*, 1655−1660.
57. Urisman, A., Molinaro, R. J., Fischer, N., Plummer, S. J., Casey, G., Klein, E. A., Malathi, K., Magi-Galluzzi, C., Tubbs, R. R., Ganem, D., Silverman, R. H., and DeRisi, J. L. (2006) Identification of a novel Gammaretrovirus in prostate tumors of patients homozygous for R462Q RNASEL variant, *PLoS. Pathog. 2*, e25.
58. Allain, B., Lapadat-Tapolsky, M., Berlioz, C., and Darlix, J. L. (1994) Transactivation of the minus-strand DNA transfer by nucleocapsid protein during reverse transcription of the retroviral genome, *EMBO J. 13*, 973−981.
59. Allain, B., Rascle, J. B., de Rocquigny, H., Roques, B., and Darlix, J. L. (1998) CIS elements and trans-acting factors required for minus strand DNA transfer during reverse transcription of the genomic RNA of murine leukemia virus, *J. Mol. Biol. 277*, 225−235.
60. Cupelli, L., Okenquist, S. A., Trubetskoy, A., and Lenz, J. (1998) The secondary structure of the R region of a murine leukemia virus is important for stimulation of long terminal repeat-driven gene expression, *J. Virol. 72*, 7807−7814.
61. Mougel, M., Tounekti, N., Darlix, J. L., Paoletti, J., Ehresmann, B., and Ehresmann, C. (1993) Conformational analysis of the 5′ leader and the gag initiation site of Mo-MuLV RNA and allosteric transitions induced by dimerization, *Nucleic Acids Res. 21*, 4677−4684.
62. De Rocquigny, H., Ficheux, D., Gabus, C., Fournie-Zaluski, M. C., Darlix, J. L., and Roques, B. P. (1991) First large scale chemical synthesis of the 72 amino acid HIV-1 nucleocapsid protein NCp7 in an active form, *Biochem. Biophys. Res. Commun. 180*, 1010−1018.
63. Beltz, H., Piemont, E., Schaub, E., Ficheux, D., Roques, B., Darlix, J. L., and Mely, Y. (2004) Role of the structure of the top half of

HIV-1 cTAR DNA on the nucleic acid destabilizing activity of the nucleocapsid protein NCp7, *J. Mol. Biol. 338*, 711−723.
64. Bernacchi, S., Stoylov, S., Piemont, E., Ficheux, D., Roques, B. P., Darlix, J. L., and Mely, Y. (2002) HIV-1 nucleocapsid protein activates transient melting of least stable parts of the secondary structure of TAR and its complementary sequence, *J. Mol. Biol. 317*, 385−399.
65. Livesey, A. K., and Brochon, J. C. (1987) Analyzing the distribution of decay constants in pulse-fluorimetry using the maximum entropy method, *Biophys. J. 52*, 693−706.
66. Clamme, J. P., Azoulay, J., and Mely, Y. (2003) Monitoring of the formation and dissociation of polyethylenimine/DNA complexes by two photon fluorescence correlation spectroscopy, *Biophys. J. 84*, 1960−1968.
67. Thompson, N. L. (1991) Fluorescence correlation spectroscopy, in *Topics in Fluorescence Spectroscopy* (Lakowicz, J. R., Ed.) pp 337−378, Plenum Press, New York.
68. Azoulay, J., Clamme, J. P., Darlix, J. L., Roques, B. P., and Mely, Y. (2003) Destabilization of the HIV-1 complementary sequence of TAR by the nucleocapsid protein through activation of conformational fluctuations, *J. Mol. Biol. 326*, 691−700.
69. Beltz, H., Azoulay, J., Bernacchi, S., Clamme, J. P., Ficheux, D., Roques, B., Darlix, J. L., and Mely, Y. (2003) Impact of the terminal bulges of HIV-1 cTAR DNA on its stability and the destabilizing activity of the nucleocapsid protein NCp7, *J. Mol. Biol. 328*, 95−108.
70. Schuler, W., Dong, C., Wecker, K., and Roques, B. P. (1999) NMR structure of the complex between the zinc finger protein NCp10 of Moloney murine leukemia virus and the single-stranded pentanucleotide d(ACGCC): comparison with HIV-NCp7 complexes, *Biochemistry 38*, 12984−12994.
71. Bombarda, E., Ababou, A., Vuilleumier, C., Gerard, D., Roques, B. P., Piemont, E., and Mely, Y. (1999) Time-resolved fluorescence investigation of the human immunodeficiency virus type 1 nucleocapsid protein: influence of the binding of nucleic acids, *Biophys. J. 76*, 1561−1570.
72. Egele, C., Schaub, E., Ramalanjaona, N., Piemont, E., Ficheux, D., Roques, B., Darlix, J. L., and Mely, Y. (2004) HIV-1 nucleocapsid protein binds to the viral DNA initiation sequences and chaperones their kissing interactions, *J. Mol. Biol. 342*, 453−466.
73. Vuilleumier, C., Bombarda, E., Morellet, N., Gerard, D., Roques, B. P., and Mely, Y. (1999) Nucleic acid sequence discrimination by the HIV-1 nucleocapsid protein NCp7: a fluorescence study, *Biochemistry 38*, 16816−16825.
74. Montenay-Garestier, T., Toulme, F., Fidy, J., Toulme, J.-J., and Le Doan, T. (1983) in *Structure, Dynamics and Interactions and Evolution of Biological Macromolecules* (Helene, C., Ed.) pp 113−128, D. Reidel Publishing Co., Dordrecht, The Netherlands.
75. Fisher, R. J., Rein, A., Fivash, M., Urbaneja, M. A., Casas-Finet, J. R., Medaglia, M., and Henderson, L. E. (1998) Sequence-specific binding of human immunodeficiency virus type 1 nucleocapsid protein to short oligonucleotides, *J. Virol. 72*, 1902−1909.
76. Bernacchi, S., and Mely, Y. (2001) Exciton interaction in molecular beacons: a sensitive sensor for short range modifications of the nucleic acid structure, *Nucleic Acids Res. 29*, E62.
77. Fisher, R. J., Fivash, M. J., Stephen, A. G., Hagan, N. A., Shenoy, S. R., Medaglia, M. V., Smith, L. R., Worthy, K. M., Simpson, J. T., Shoemaker, R., McNitt, K. L., Johnson, D. G., Hixson, C. V., Gorelick, R. J., Fabris, D., Henderson, L. E., and Rein, A. (2006) Complex interactions of HIV-1 nucleocapsid protein with oligonucleotides, *Nucleic Acids Res. 34*, 472−484.
78. Stoylov, S. P., Vuilleumier, C., Stoylova, E., De Rocquigny, H., Roques, B. P., Gerard, D., and Mely, Y. (1997) Ordered aggregation of ribonucleic acids by the human immunodeficiency virus type 1 nucleocapsid protein, *Biopolymers 41*, 301−312.
79. Hess, S. T., Huang, S., Heikal, A. A., and Webb, W. W. (2002) Biological and chemical applications of fluorescence correlation spectroscopy: a review, *Biochemistry 41*, 697−705.
80. Bonnet, G., Krichevsky, O., and Libchaber, A. (1998) Kinetics of conformational fluctuations in DNA hairpin-loops, *Proc. Natl. Acad. Sci. U.S.A. 95*, 8602−8606.
81. Dey, A., York, D., Smalls-Mantey, A., and Summers, M. F. (2005) Composition and sequence-dependent binding of RNA to the nucleocapsid protein of Moloney murine leukemia virus, *Biochemistry 44*, 3735−3744.
82. D'Souza, V., and Summers, M. F. (2004) Structural basis for packaging the dimeric genome of Moloney murine leukaemia virus, *Nature 431*, 586−590.
83. Casas-Finet, J. R., Jhon, N. I., and Maki, A. H. (1988) p10, a low molecular weight single-stranded nucleic acid binding protein of murine leukemia retroviruses, shows stacking interactions of its single tryptophan residue with nucleotide bases, *Biochemistry 27*, 1172−1178.
84. Gorelick, R. J., Henderson, L. E., Hanser, J. P., and Rein, A. (1988) Point mutants of Moloney murine leukemia virus that fail to package viral RNA: evidence for specific RNA recognition by a "zinc finger-like" protein sequence, *Proc. Natl. Acad. Sci. U.S.A. 85*, 8420−8424.
85. Yu, Q., and Darlix, J. L. (1996) The zinc finger of nucleocapsid protein of Friend murine leukemia virus is critical for proviral DNA synthesis in vivo, *J. Virol. 70*, 5791−5798.
86. Gorelick, R. J., Chabot, D. J., Ott, D. E., Gagliardi, T. D., Rein, A., Henderson, L. E., and Arthur, L. O. (1996) Genetic analysis of the zinc finger in the Moloney murine leukemia virus nucleocapsid domain: replacement of zinc-coordinating residues with other zinc-coordinating residues yields noninfectious particles containing genomic RNA, *J. Virol. 70*, 2593−2597.
87. Demene, H., Dong, C. Z., Ottmann, M., Rouyez, M. C., Jullian, N., Morellet, N., Mely, Y., Darlix, J. L., Fournie-Zaluski, M. C., Saragosti, S., et al. (1994) 1H NMR structure and biological studies of the His23→Cys mutant nucleocapsid protein of HIV-1 indicate that the conformation of the first zinc finger is critical for virus infectivity, *Biochemistry 33*, 11707−11716.
88. Ramboarina, S., Morellet, N., Fournie-Zaluski, M. C., and Roques, B. P. (1999) Structural investigation on the requirement of CCHH zinc finger type in nucleocapsid protein of human immunodeficiency virus 1, *Biochemistry 38*, 9600−9607.
89. Stote, R. H., Kellenberger, E., Muller, H., Bombarda, E., Roques, B. P., Kieffer, B., and Mely, Y. (2004) Structure of the His44 → Ala single point mutant of the distal finger motif of HIV-1 nucleocapsid protein: a combined NMR, molecular dynamics simulation, and fluorescence study, *Biochemistry 43*, 7687−7697.
90. Williams, M. C., Gorelick, R. J., and Musier-Forsyth, K. (2002) Specific zinc-finger architecture required for HIV-1 nucleocapsid protein's nucleic acid chaperone function, *Proc. Natl. Acad. Sci. U.S.A. 99*, 8614−8619.
91. Kanevsky, I., Chaminade, F., Ficheux, D., Moumen, A., Gorelick, R., Negroni, M., Darlix, J. L., and Fosse, P. (2005) Specific interactions between HIV-1 nucleocapsid protein and the TAR element, *J. Mol. Biol. 348*, 1059−1077.
92. Vo, M. N., Barany, G., Rouzina, I., and Musier-Forsyth, K. (2006) Mechanistic studies of mini-TAR RNA/DNA annealing in the absence and presence of HIV-1 nucleocapsid protein, *J. Mol. Biol. 363*, 244−261.
93. Druillennec, S., and Roques, B. P. (2000) HIV-1 NCp7 as a target for the design of novel antiviral agents, *Drug News Perspect. 13*, 337−349.

BI7012239